

A new technique for bearing fault detection in the time-frequency domain

Behrooz Attaran, Afshin Ghanbarzadeh * and Shapour Moradi

Mechanical Engineering Department, Shahid Chamran University of Ahvaz, Ahvaz, Iran

ARTICLE INFO

Article history:

Received: 24 May 2019

Accepted: 11 September 2019

Keywords:

Fast Kurtogram

Bearing fault detection

Statistical features

Time-Frequency domain

ABSTRACT

This paper presents a new Fast Kurtogram Method in the time-frequency domain using novel types of statistical features instead of the kurtosis. For this study, the problem of four classes for Bearing Fault Detection is investigated using various statistical features. This research is conducted in four stages. At first, the stability of each feature for each fault mode is investigated. Then, resistance to load changes as well as failure growth is studied. In the end, the resolution and fault detection for each feature using comparison with a determined pattern and the coherence rate is calculated. From the above results, the best feature that is both resistant and repeatable to different variations, as well as having suitable accuracy of detection and resolution, is selected. It is found that kurtosis feature is not in a good condition in comparison with other statistical features such as harmmean and median. This approach increases the fault identification accuracy significantly.

1. Introduction

The desire and need for precision detection capabilities and precautionary predictions have long been equivalent to human use of complex and expensive machines. Efforts to develop and implement varying degrees of detection and anticipation capabilities have a long history. Exploiting rotary machines is one of the major challenges in maintenance and repair. Intelligent maintenance and repair, as well as diagnosis and prediction of deficiencies, are essential for the oil, gas, refinery, petrochemical, transportation, aerospace, military and commercial vessels, automation and other industries. Diagnosing and anticipating defects is one of the challenging issues of the health management system and the anticipation of modern defects. Reduces the cost of support and operation, as well as the total cost of ownership over the life cycle, and improves the level of safety of many types of machinery and complex systems. The evolution of fault diagnostic monitoring systems for rotating equipment and other complex systems helps to realize that it is possible to identify predictive defects desirable and technically possible. The most important challenge is addressing the signal of roller bearing defects. Bearing defects are produced in the form of blows caused by passing roll elements on the surface of the failure. Identifying and monitoring these flaws is difficult, especially in the early stages of the defect, which is a very small failure and is easily covered with other components. Undoubtedly, all defect prediction techniques need to be further developed to better adapt to the characteristics of nonlinear systems so that they can be used in real-world conditions. Yang et al. [1] used a new time-frequency domain called base track that was recently created. In fact, they used the application of this new method to extract the characteristics of the faulty roller bearing signals with internal and external cannon

failures. In the following, the results of this method were compared with the results of the discrete Wavelet packet analysis method and the follow-up matching technique and showed that the failure characteristics of the base tracking technique create a better resolution in the time-frequency domain. Therefore, the analysis and interpretation of the results will be simplified. It also improves the ratio of noise to the signal.

In [2], Liang and Bochalooi proposed an energy operator method for frequency and domain division and showed that the Tiger energy operator is suitable for extracting the frequency modulation and the amplitude of the vibrational signals of mechanical systems. Due to the continuity of frequency modulation information in this method, there is no need for multiple steps to remove unwanted components. So that the range of diamonds inherently in the energy operator can determine the failure frequency from the energy spectrum of the energy conversion. Another advantage of this method is the lack of choice of parameters. Suu et al. [3] presented a new compound-based Morellet wavelet filtering method that improves self-dependency. Initially, in order to eliminate the frequency of interference vibrations, the vibration signal is filtered by the midpoint filter specified by the Morellet wavelet. Also, the parameters associated with the Morellet wavelet, including the central frequency and bandwidth, are optimized by the genetic algorithm, whose target function is the minimization criterion for Shannon entropy. In order to further reduce the residual noise in the band and to highlight intermittent traits, the self-correlation amplification algorithm is used for signal filtering. Doo et al. In [4], a new intelligent method for diagnosing rotary machines based on intrinsic mode decomposition, dimensional parameters, decomposition table, law inference algorithm called second

editing tutorial for modified modules examples and modified strategy for implementing the presentation law have given. The EMD method for preprocessing vibrating signals is used to accurately derive the characteristics of the failure. Then, the non-dimensional parameters extracted from the decomposed signals in the time domain and the Enolop spectrum in the frequency domain are obtained for the decomposition table. The MLEM2 algorithm is then executed on the fail decision table for producing decision rules. Finally, the IRMS method is classified.

Lee et al. [5] presented a new classifier based on the lattice framework for the classification of the friction grid for the problem of detecting bearing defects. This method does not need to determine any parameters and converges at a high speed with a small number of inference law. To illustrate the results, they used five datasets, and ultimately demonstrated their efficiency and accuracy compared to the same method of fuzzy network argumentation and other neural networks.

Wang et al. [6] presented the advanced Kurtogram method for detecting roller bearing defects. The decoder is based on the elongation of the time signals that are filtered by the Fourier transform. Also, the transformation of the wavelet packet is also used as a substitute for the Fourier transform of the short time to analyze the signal in this method. However, the elongation of time signals is useful in some cases but is poorly performed when the signal-to-noise ratio is low or non-Gaussian noise. Therefore, they proposed a high-performance encoder based on the amplitude power of the signals extracted from the wavelet packet. This method helps in determining the location of frequency amplification bands for further modulation. Finally, the frequency characteristics of the ANOLOP signal are used to determine the type of bearing failure .

In [7], Zhou and Chen provided an intelligent diagnostic method for rolled bearings based on the least squares of the back propagation machine optimized by the modified particle optimization method. In this method, first, the initial vibration signals are decomposed into several intrinsic mode functions, which is done by the EMD method and the energy attribute values extracted based on the energy-entropy of the IMF. Finally, the energy indicators extracted as breakdown property vectors, the IPSO-LSSVM classifier inputs, are used to identify the different failure patterns.

In [8], Albuagbi and Trondaphilova presented a method for identifying roller bearing defects. Their method consists of two main steps. Pretreatment of signals, based on several signal analysis algorithms and defect detection, which uses the pattern recognition process. The first step is, in fact, linear time constant based on automated modeling of regression. In the pre-purification step, the spectral analysis method is used to remove noise from the signal. They used three different sets of labs to validate the proposed method to detect various types of roller bearings.

In [9], Baraldi and colleagues presented a method to identify the beginning of a failure, to detect defective bearings in the system, to classify the type of failure, and to determine the severity of the failure. Their fault diagnosis is based on the hierarchical structure associated with the classification of the nearest neighbor K. Feature Selection The vibration signals for the input of the fault diagnostic system are based on the packaging method based on the multi-objective optimization integrated with the binary differential algorithm and the KNN classifier.

In [10], Vakharia et al. Presented an algorithm for detecting various bearing defects of measured vibrational signals. Characteristics such as elongation, squaring, mean, root mean

squares, or more complex features such as Shannon entropy from the time domain, frequency domain, and discrete wavelet transform are calculated. This feature takes on all bearings, including bearings, defective interior faults, defective balls, and faulty external censuses. Feature rating methods such as Qi square and Assist-F method are used to select the best feature. Their results showed that this method would reduce the feature vector collection used for the classifier.

In [11], Singh et al. presented an algorithm based on a flexible, logically complementary wavelet transform. Their method in frequency segmentation is flexible to produce a number of filters with a variety of bandwidths. The optimal filter selection, which is completely overlapping with bearing defects in the excited region, is performed based on the maximum amount of shock detection provided by the "self-bonding elongation of the intermediate energy" function. The offered index was robust and consistent in evaluating impulsive failure signals in the presence of interference vibrations such as heavy background noise or sporadic shock. Their methods are also sensitive to breakdown severity.

Yaylı [12] conveniently computed an accurate buckling parameter for microbeams using both classical and non-classical boundary conditions restrained by translational and rotational springs.

The main objective of [13] was to present a general analytical approach for the dynamical analysis of nanorods (carbon nanotubes) with arbitrary boundary conditions (restrained or rigid).

In [14] The buckling characteristics of elastically restrained embedded microbeams were investigated in some numerical examples. There were very good agreements between this study and the previous results indicating the validity of the presented method.

In [15], torsional dynamics of nanotubes embedded in an elastic medium with arbitrary elastic boundary conditions was studied. The proposed mathematical model developed based on the nonlocal elasticity theory gives us opportunity to include small-scale parameter. Two springs in torsional direction were attached to a nanotube at both boundaries.

In [16], torsional vibration analysis of carbon nano tubes with general elastic boundary conditions was presented via modified couple stress theory. The model developed based on modified couple stress theory gives us opportunity to interpret small size effect. Two torsional springs were attached to a single-walled carbon nanotube at both ends. The idea of the proposed work was to obtain a coefficient matrix for eigen-value analysis involving the torsional spring coefficients.

In [17], the vibration analysis of composite natural gas pipeline in the thermal and humidity environment was studied. The effect of the non-uniform magnetic field was investigated. The equation of motion was derived by applying the Hamilton's principle for the pipe with the effects of both linear and nonlinear stress temperature cases.

In [18], The updating process used an evolutionary optimization algorithm, namely bees algorithm which applied instinctive behavior of honeybees for finding food sources. To determine the uncertain updated parameters such as geometry and material properties of the structure, local and global sensitivity analyses had been performed. The sum of the squared errors between the natural frequencies obtained from operational modal analysis and the finite element method was used to define the objective function.

In [19], the free vibration behavior of nanoscale FG rectangular plates was studied within the framework of the refined plate theory (RPT) and small-scale effects were taken into account. Using the nonlocal elasticity theory, the governing equations were derived for single-layered FG nanoplate. The Navier's method was employed to obtain closedform solutions for rectangular nanoplates assuming that all edges were simply supported.

In [20], wave propagation approach was used to analysis the free vibration and buckling analysis of the thick rectangular plates based on higher order shear deformation plate theory. From wave viewpoint, vibrations can be considered as travelling waves along structures.

In [21], the wave propagation method was combined with nonlocal elasticity theory to analyze the buckling and free vibration of rectangular Reddy nanoplate. Wave propagation was one of the powerful methods for analyzing the vibration and buckling of structures. It was assumed that the plate has two opposite edges simply supported while the other two edges may be simply supported or clamped.

In [22], a mathematical model to investigate the behaviour of adaptable shock absorber dynamics for the six-degree-of-freedom aircraft model in the taxiing phase was developed. The purpose of this research was to design a proportional-integral-derivative technique for control of an active vibration absorber system using a hydraulic nonlinear actuator based on the bees algorithm.

In [23], the coefficients of controller, the parameters of hydraulic nonlinear actuator added to the traditional shock absorber system, and the vibration absorber were optimized simultaneously by the bee intelligent multi-objective algorithm. As well as, for proving adaptability of this algorithm, this paper presented the sensitivity analysis of three point landing due to the additional payload and the touchdown speed and the robustness analysis of one and two point landings due to the wind conditions as emergency situation on the runway as an innovated work.

The proposed method of this research is based on kurtogram. The novelty of the present work in comparison with previous published articles in the literature is that against of using kurtosis feature in kurtogram method, it utilizes new statistical features. Then, instead of diagnosis based on kurtogram output analytically, fault diagnostics is performed according to the patterns of each failure. The fault identification accuracy may be increased by this approach.

In this research, first an introduction is described in chapter 1. Then in chapter 2, kurtogram method is explained. Chapter 3 describes an experimental setup for validation of this work. Chapter 4 represents the proposed approach of this paper in details, and chapter 5 covers conclusion and the future work.

2. Kurtogram

Despite the benefits of wavelet transformation, challenges include choosing the right mother-wavelet from a variety of examples, as well as high computational costs, especially for smaller scale levels. These challenges have suggested different ways to improve the wavelet transform or different ways to select the appropriate wavelet. Some of these improvements are mentioned in previous studies. On the other hand, these challenges in the transformation of the wavelet have led to the emergence of other methods, such as the spectral kurtosis and Kurtogram.

The Kurtogram method is based on the Spectral Kurtosis, which is a high-order statistical method. In 1983, the first use of the frequency spectrum was carried out by Dewey. In the

following years, this method quickly progressed and improved for a variety of applications. Then, Anthony proposed in 2004 the elongation based on the Vold-Cramer decomposition, which described each non-terminal signal as the output of a variable-time linear system.

In [24], ensemble machine learning techniques were demonstrated for the detection of different AFB faults. Initially, statistical features were extracted from temporal vibration signals and were collected using experimental test rig for different input parameters like load, speed and bearing conditions. [25] proposed a reduct construction method based on discernibility matrix simplification. The method worked with the genetic algorithm. To identify potential problems and prevent complete failure of bearings, a new method based on rule-based classifier ensemble was presented.

Li et al. [26] focused on the problem of accurate Fault Characteristic Frequency (FCF) estimation of the rolling bearing. Teager-Kaiser Energy Operator (TKEO) demodulation has been applied widely to rolling bearing fault detection. FCF could be extracted from vibration signals, which was pre-treatment by TKEO demodulation method.

In the further development of the Kurtogram in 2018 [27], Musharrafzadeh and Fassana showed that, despite the capabilities of the QuickTech method, however, when the signal-to-noise ratio is very low or the presence of non-voiced noise, the performance of the choreographer's method drops significantly; therefore, the autogram method is introduced. Which is largely similar to the same method, with the difference that the calculation of the elongation based on the self-correlation of the signal obtained from the Enolop square in the frequency bands, which partially succeeded in increasing the accuracy of the failure detection and lowering the computational cost [28],[29].

So according to the above, new methods such as Spectral Kurtosis, Fast Kurtogram, Autogram have been developed to replace the wavelet. All of these methods are based on the statistic feature of the kurtosis. In this study, a new time-frequency domain was introduced, and other commonly statistical features are used instead of the Kurtosis feature. The proposed process is as follows:

1. Design of low pass and high pass filters for binary decomposition, as well as the design of low pass, band-pass and high pass filters for ternary of signal analysis
2. The signal once decomposed into binary and ternary, then each section of the binary decomposition is again degraded the again binary and ternary, and the same trend continues for higher decomposition levels.
3. Calculate common features for each section obtained from the previous step for comparison
4. Choosing the proper features

For this purpose, the feature should be chosen so that the time-frequency domain derives from the following conditions :

Firstly, the time-frequency domain must be robust and repeatable for failure with specified type and severity. That is, different measured signals for a failure type provide the same time-frequency domain .

Secondly, the time-frequency domain for each fault mode must be resilient and repeatable to changes in conditions such as load change. That is, with different loads, the same time-frequency domain is achieved .

Third, the time-frequency domain for each failure is robust and repeatable against of the growth failure. In other words, in the case of breakdowns with different depths, but of the same type, the time-frequency domain presents a relatively similar behavior .

Fourth, the ability to detect and differentiate the time-frequency domain of each feature is appropriate for various failures.

Below are the statistical features that are being studied in this study:

Data samples can have thousands (even millions) of values. Descriptive statistics can summarize these data into a few numbers that contain most of the relevant information. The Following statistical parameters are used to detect incipient bearing damage: root mean square, interquartile range, skewness, mean, Geometric mean, harmonic mean, mean excluding outliers, largest element, smallest element, most frequent value, standard deviation, variance, median, range, sum, trapezoidal integration, mean absolute deviation, moment and percentiles.

where X_i ($i=1, \dots, N$) is the amplitude at sampling point i and N is the number of sampling points. μ is the mean of X , σ is the standard deviation of X , and $E(.)$ represents the mathematical expectation.

3. Experimental setup

The vibration data used in this study were obtained from the dataset of the rolling element bearings under different operating loads and bearing conditions according to Table 1. The ball bearings are installed in a motor-driven mechanical system. A 2-hp, the three-phase induction motor is connected to a dynamometer and a torque sensor by a self-aligning coupling. The dynamometer is controlled so that the desired torque load levels can be achieved. An accelerometer, with a frequency range of 20-20 kHz is mounted on the motor housing at the drive end of the motor to acquire the vibration signals from the bearing. The data collection system consists of a high-bandwidth amplifier particularly designed for the vibration signals and a data recorder with a sampling frequency of 12 kHz per channel. The bearings used in this study are deep groove ball bearings manufactured by SKF. The faults were introduced into the drive-end bearing of the motor using the electro-discharge machining method. The defect size (diameter, depth) of the three faults was the same, 0.007", 0.014", 0.021" and 0.028". Each bearing was tested under four different loads, (e.g. 0, 1, 2, and 3 hp corresponding to 0, 0.736, 1.491, and 2.237 kW). The motor speed during the experimental tests was 1720-1797 r/min. The bearing dataset was obtained from the experimental system under the four different operating conditions: (1) normal condition; (2) Inner race fault; (3) Ball fault; and (4) Outer race fault [4].

In order to develop a robust fault diagnosis model that is able to identify the existence of different faults under varying load conditions, and to evaluate the proposed methods, this fault diagnosis problem is set as a four-class classification problem [4].

4. Results discussion

4.1. First stage

First, the resistance of the time-frequency domain of each figure must be checked for any specific failure. For this purpose, ten raw signals are considered for each mode, then using one of the introduced features, the time-frequency domain is calculated and the resulting matrix is normalized. Finally, the standard deviation of ten time-frequency domains is calculated relative to each other.

The lower standard deviation leads to be more robust and repeatable of the time-frequency domain.

In Table 2, anyone whose total rank is less than that, the time-frequency domain resulting from it is more resistant and more repeatable. As you can see, the feature of kurtosis in this comparison is not good.

Table 1. Bearing dataset of Case Western Reserve University

| Fault Diameter | Motor Load (HP) | Motor Speed (rpm) | Normal | Inner Race | Ball | Outer Race |
|----------------|-----------------|-------------------|--------|------------|--------|------------|
| Normal | 0 | 1797 | Class1 | * | * | * |
| | 1 | 1772 | | * | * | * |
| | 2 | 1750 | | * | * | * |
| | 3 | 1730 | | * | * | * |
| 0.007" | 0 | 1797 | * | Class2 | Class3 | Class4 |
| | 1 | 1772 | * | | | |
| | 2 | 1750 | * | | | |
| | 3 | 1730 | * | | | |
| 0.014" | 0 | 1797 | * | Class2 | Class3 | Class4 |
| | 1 | 1772 | * | | | |
| | 2 | 1750 | * | | | |
| | 3 | 1730 | * | | | |
| 0.021" | 0 | 1797 | * | Class2 | Class3 | Class4 |
| | 1 | 1772 | * | | | |
| | 2 | 1750 | * | | | |
| | 3 | 1730 | * | | | |
| 0.028" | 0 | 1797 | * | Class2 | Class3 | Class4 |
| | 1 | 1772 | * | | | |
| | 2 | 1750 | * | | | |
| | 3 | 1730 | * | | | |

Table 2. The stability of each feature for each fault mode

| No | Feature | Inner race (std) | Rank1 | Ball fault (std) | Rank2 | Outer race (std) | Rank 3 |
|----|----------|------------------|-------|------------------|-------|------------------|--------|
| 1 | Kurtosis | 1.039 | 18 | 2.242 | 19 | 0.722 | 16 |
| 2 | Rms | 0.134 | 8 | 0.103 | 3 | 0.074 | 4 |
| 3 | IQR | 0.299 | 13 | 0.289 | 11 | 0.398 | 12 |
| 4 | Skewness | 1.401 | 20 | 2.382 | 20 | 0.911 | 19 |
| 5 | Mean | 0.194 | 11 | 0.109 | 5 | 0.141 | 10 |
| 6 | Geomean | 0.350 | 15 | 0.253 | 10 | 0.768 | 17 |
| 7 | Harmmean | 0.993 | 17 | 0.922 | 16 | 0.524 | 13 |
| 8 | Trimmean | 0.257 | 12 | 0.136 | 6 | 0.620 | 14 |
| 9 | Max | 0.134 | 9 | 0.465 | 14 | 0.118 | 8 |
| 10 | Min | 0.641 | 16 | 0.937 | 17 | 0.896 | 18 |
| 11 | Mode | 1.363 | 19 | 1.295 | 18 | 1.128 | 20 |
| 12 | Std | 0.090 | 5 | 0.187 | 9 | 0.090 | 5 |
| 13 | Var | 0.049 | 3 | 0.105 | 4 | 0.036 | 3 |
| 14 | Median | 0.315 | 14 | 0.357 | 12 | 0.637 | 15 |
| 15 | Range | 0.144 | 10 | 0.467 | 15 | 0.114 | 7 |
| 16 | Sum | 0.005 | 1 | 0.008 | 1 | 0.006 | 1 |
| 17 | Trapz | 0.005 | 2 | 0.008 | 2 | 0.006 | 2 |
| 18 | Mad | 0.096 | 6 | 0.172 | 8 | 0.120 | 9 |
| 19 | Moment | 0.084 | 4 | 0.162 | 7 | 0.101 | 6 |
| 20 | Prctile | 0.131 | 7 | 0.381 | 13 | 0.146 | 11 |

4.2. Second stage

At this stage, the resistance of the time-frequency domain to the change in load must be checked. For this purpose, for each of the three types of failure, four magnitudes of the load are considered, and after using the time-frequency domain statistical features, the normalization process is performed and then, the standard deviation of the four time-frequency domains is calculated. Eventually, any feature whose total deviation is less than normal will naturally be more resistant to detecting the failure mode according to Table 3.

Table 3. Resistance of each feature to load change

| No | Feature | Inner race (std) | rank1 | Ball fault (std) | rank2 | Outer race (std) | rank3 |
|----|----------|------------------|-------|------------------|-------|------------------|-------|
| 1 | Kurtosis | 1.092 | 19 | 2.636 | 19 | 0.450 | 12 |
| 2 | Rms | 0.342 | 9 | 0.218 | 9 | 0.144 | 6 |
| 3 | IQR | 0.405 | 12 | 0.234 | 12 | 0.642 | 15 |
| 4 | skewness | 0.762 | 18 | 2.653 | 20 | 0.515 | 13 |
| 5 | Mean | 0.378 | 11 | 0.227 | 11 | 0.238 | 11 |
| 6 | Geomean | 0.594 | 15 | 0.236 | 13 | 1.968 | 20 |
| 7 | harmmean | 0.561 | 14 | 1.163 | 16 | 1.310 | 19 |
| 8 | trimmean | 0.511 | 13 | 0.215 | 8 | 0.672 | 16 |
| 9 | Max | 0.339 | 7 | 0.299 | 14 | 0.151 | 8 |
| 10 | Min | 0.599 | 16 | 1.761 | 18 | 0.555 | 14 |
| 11 | Mode | 1.193 | 20 | 1.509 | 17 | 0.918 | 17 |
| 12 | Std | 0.279 | 5 | 0.171 | 5 | 0.103 | 4 |
| 13 | Var | 0.223 | 4 | 0.102 | 3 | 0.060 | 3 |
| 14 | Median | 0.636 | 17 | 0.203 | 7 | 0.956 | 18 |
| 15 | Range | 0.342 | 10 | 0.301 | 15 | 0.173 | 9 |
| 16 | Sum | 0.019 | 2 | 0.015 | 1 | 0.012 | 2 |
| 17 | Trapz | 0.019 | 1 | 0.015 | 2 | 0.012 | 1 |
| 18 | Mad | 0.341 | 8 | 0.178 | 6 | 0.187 | 10 |
| 19 | Moment | 0.332 | 6 | 0.168 | 4 | 0.147 | 7 |
| 20 | Prctile | 0.213 | 3 | 0.222 | 10 | 0.112 | 5 |

4.3. Third stage

In this section, it is necessary to select a feature that the time-frequency domain resulting from it will not fail against the growth of the failure and is still resistant and will not fail with other types of failure. For this purpose, for each failure, four growth stages are considered and ultimately the standard deviation of the four time-frequency domains obtained for each feature is calculated and the results are presented in Table 4.

Table 4. Resistance of each feature to failure growth

| No | Feature | Inner race (std) | rank1 | Ball fault (std) | rank2 | Outer race (std) | rank3 |
|----|----------|------------------|-------|------------------|-------|------------------|-------|
| 1 | Kurtosis | 3.614 | 20 | 3.323 | 20 | 5.262 | 19 |
| 2 | Rms | 0.625 | 10 | 0.398 | 8 | 0.464 | 5 |
| 3 | IQR | 1.120 | 13 | 0.415 | 10 | 3.880 | 18 |
| 4 | Skewness | 3.522 | 19 | 2.779 | 19 | 5.585 | 20 |
| 5 | Mean | 0.798 | 11 | 0.607 | 12 | 0.564 | 6 |
| 6 | Geomean | 1.451 | 16 | 1.068 | 15 | 3.591 | 16 |
| 7 | harmmean | 1.249 | 15 | 1.147 | 17 | 3.230 | 15 |
| 8 | trimmean | 1.020 | 12 | 0.834 | 13 | 2.216 | 14 |
| 9 | Max | 0.387 | 4 | 0.317 | 4 | 0.256 | 3 |
| 10 | Min | 1.156 | 14 | 1.444 | 18 | 0.569 | 7 |
| 11 | Mode | 1.505 | 17 | 1.100 | 16 | 1.838 | 13 |
| 12 | Std | 0.541 | 6 | 0.415 | 11 | 1.090 | 10 |
| 13 | Var | 0.425 | 5 | 0.318 | 6 | 0.754 | 9 |
| 14 | Median | 1.542 | 18 | 1.027 | 14 | 3.867 | 17 |
| 15 | Range | 0.377 | 3 | 0.316 | 3 | 0.256 | 4 |
| 16 | Sum | 0.067 | 2 | 0.052 | 2 | 0.076 | 2 |
| 17 | Trapz | 0.067 | 1 | 0.052 | 1 | 0.076 | 1 |
| 18 | Mad | 0.555 | 7 | 0.379 | 7 | 1.518 | 12 |
| 19 | Moment | 0.576 | 8 | 0.400 | 9 | 1.374 | 11 |
| 20 | Prctile | 0.582 | 9 | 0.317 | 5 | 0.722 | 8 |

4.4. Fourth stage

In this phase, the decomposability of the failures is investigated using the time-frequency domain derived from different statistical features. For this purpose, for each failure, a time-frequency domain is already considered as a pattern, and then for each new signal, it receives the corresponding time-frequency domain and compares with the four previous patterns. Coherence has been used to calculate the similarity of each time-frequency domain with patterns. The coherence number is closer to one, the two are more similar, and it approaches zero, they are more different.

The Tables 5a,b has two parts; first, each breakdown is compared to its own pattern, the sum of which is the True column. Then, the similarity of each failure with the other failure patterns is compared, and their sum is also the False column. Now the feature is appropriate to have a greater True value and simultaneously the False value is low. For this review, the Tables 5a,b is presented in Figure 1.

Table 5a. Comparison with a pattern and the coherence rate

| No | Feature | (1,1) | (2,2) | (3,3) | (4,4) | True (Sum) | (1,2) | (1,3) |
|----|----------|-------|-------|-------|-------|------------|-------|-------|
| 1 | kurtosis | 0.49 | 0.73 | 0.40 | 0.84 | 2.45 | 0.15 | 0.37 |
| 2 | Rms | 1.00 | 1.00 | 0.98 | 1.00 | 3.98 | 0.23 | 0.27 |
| 3 | IQR | 0.99 | 0.94 | 0.90 | 0.99 | 3.81 | 0.22 | 0.27 |
| 4 | skewness | 0.44 | 0.56 | 0.41 | 0.54 | 1.95 | 0.28 | 0.35 |
| 5 | Mean | 1.00 | 1.00 | 0.98 | 1.00 | 3.98 | 0.24 | 0.27 |
| 6 | geomean | 1.00 | 0.99 | 0.97 | 0.99 | 3.95 | 0.24 | 0.26 |
| 7 | harmmean | 0.98 | 0.92 | 0.90 | 0.94 | 3.74 | 0.23 | 0.23 |
| 8 | trimmean | 1.00 | 0.99 | 0.98 | 1.00 | 3.97 | 0.24 | 0.26 |
| 9 | Max | 0.98 | 0.98 | 0.95 | 1.00 | 3.91 | 0.30 | 0.29 |
| 10 | Min | 0.85 | 0.64 | 0.46 | 0.69 | 2.64 | 0.43 | 0.32 |
| 11 | Mode | 0.77 | 0.60 | 0.72 | 0.66 | 2.74 | 0.36 | 0.22 |
| 12 | Std | 0.99 | 0.99 | 0.97 | 1.00 | 3.95 | 0.24 | 0.28 |
| 13 | Var | 1.00 | 1.00 | 0.99 | 1.00 | 3.98 | 0.35 | 0.39 |
| 14 | median | 1.00 | 0.98 | 0.98 | 0.97 | 3.92 | 0.23 | 0.27 |
| 15 | Range | 0.98 | 0.98 | 0.95 | 0.99 | 3.90 | 0.30 | 0.29 |
| 16 | Sum | 1.00 | 1.00 | 1.00 | 1.00 | 4.00 | 0.66 | 0.62 |
| 17 | Trapz | 1.00 | 1.00 | 1.00 | 1.00 | 4.00 | 0.66 | 0.62 |
| 18 | Mad | 0.99 | 0.98 | 0.97 | 1.00 | 3.94 | 0.23 | 0.28 |
| 19 | moment | 0.99 | 0.99 | 0.97 | 1.00 | 3.95 | 0.23 | 0.29 |
| 20 | Prctile | 0.99 | 0.98 | 0.96 | 1.00 | 3.93 | 0.26 | 0.28 |

Table 5b. Comparison with a pattern and the coherence rate

| (1,4) | (2,1) | (2,3) | (2,4) | (3,1) | (3,2) | (3,4) | (4,1) | (4,2) | (4,3) | False (Sum) |
|-------|-------|-------|-------|-------|-------|-------|-------|-------|-------|-------------|
| 0.07 | 0.18 | 0.19 | 0.39 | 0.38 | 0.15 | 0.10 | 0.10 | 0.39 | 0.12 | 2.57 |
| 0.27 | 0.23 | 0.51 | 0.60 | 0.26 | 0.54 | 0.83 | 0.27 | 0.62 | 0.80 | 5.44 |
| 0.25 | 0.22 | 0.47 | 0.46 | 0.25 | 0.49 | 0.75 | 0.26 | 0.44 | 0.70 | 4.78 |
| 0.29 | 0.26 | 0.30 | 0.26 | 0.33 | 0.30 | 0.26 | 0.23 | 0.30 | 0.28 | 3.44 |
| 0.26 | 0.23 | 0.48 | 0.56 | 0.26 | 0.51 | 0.81 | 0.26 | 0.57 | 0.79 | 5.25 |
| 0.25 | 0.23 | 0.44 | 0.50 | 0.26 | 0.47 | 0.72 | 0.24 | 0.52 | 0.69 | 4.81 |
| 0.22 | 0.23 | 0.38 | 0.41 | 0.23 | 0.41 | 0.51 | 0.22 | 0.42 | 0.47 | 3.96 |
| 0.25 | 0.23 | 0.45 | 0.52 | 0.26 | 0.48 | 0.79 | 0.25 | 0.52 | 0.77 | 5.02 |
| 0.33 | 0.28 | 0.62 | 0.79 | 0.28 | 0.67 | 0.81 | 0.32 | 0.79 | 0.79 | 6.27 |
| 0.32 | 0.45 | 0.36 | 0.44 | 0.33 | 0.37 | 0.35 | 0.39 | 0.56 | 0.34 | 4.66 |
| 0.27 | 0.42 | 0.20 | 0.40 | 0.07 | 0.06 | 0.16 | 0.38 | 0.56 | 0.15 | 3.24 |
| 0.29 | 0.23 | 0.55 | 0.64 | 0.27 | 0.59 | 0.78 | 0.29 | 0.67 | 0.76 | 5.59 |
| 0.35 | 0.34 | 0.67 | 0.70 | 0.38 | 0.72 | 0.83 | 0.34 | 0.73 | 0.81 | 6.59 |
| 0.24 | 0.23 | 0.43 | 0.46 | 0.25 | 0.45 | 0.67 | 0.23 | 0.48 | 0.69 | 4.64 |
| 0.34 | 0.28 | 0.63 | 0.79 | 0.29 | 0.67 | 0.81 | 0.33 | 0.79 | 0.80 | 6.32 |
| 0.59 | 0.67 | 0.96 | 0.93 | 0.62 | 0.96 | 0.98 | 0.60 | 0.94 | 0.98 | 9.50 |
| 0.59 | 0.67 | 0.96 | 0.93 | 0.62 | 0.96 | 0.98 | 0.60 | 0.94 | 0.98 | 9.51 |
| 0.28 | 0.23 | 0.52 | 0.59 | 0.26 | 0.56 | 0.78 | 0.28 | 0.61 | 0.76 | 5.38 |
| 0.29 | 0.23 | 0.53 | 0.61 | 0.27 | 0.57 | 0.78 | 0.28 | 0.63 | 0.76 | 5.47 |
| 0.31 | 0.24 | 0.56 | 0.72 | 0.27 | 0.61 | 0.78 | 0.30 | 0.75 | 0.76 | 5.83 |

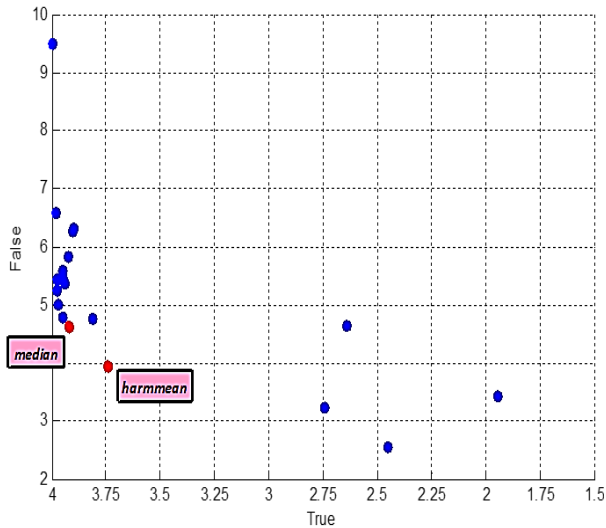


Figure 1. Coherence rate of each feature

In Figure 1, the horizontal direction is reversed for a better look. Now the feature should be selected to have a more True value and less False value, or closer to the origin of Figure 1, so the two harmmean and median features are the most appropriate ones. Figure 2 is displayed based on kurtosis feature according to [30],[31]. As you see, the first and third class, as well as the second and fourth, are relatively similar. On the other hand, as shown in the first to third tables, this feature has less resistance and repeatability in contrast to the change in load and the growth of the failure and even in a certain fault. Figure 3 is derived using the harmmean feature. This figure shows that all four classes are different, and the time-frequency domains of each fault with its failure pattern match entirely. On the other hand, in the tables of the first stage to the third stage can be perceived as a good repeatability status against load change and deterioration.

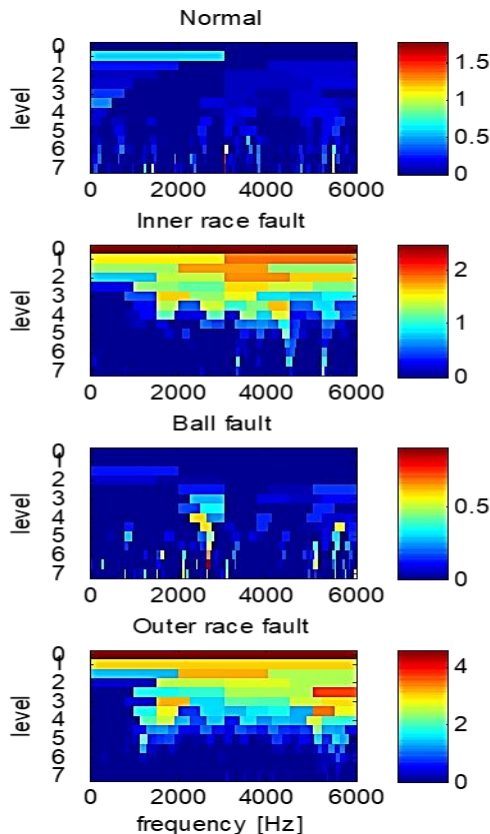


Figure 2. The Fast Kurtogram [19] using kurtosis feature

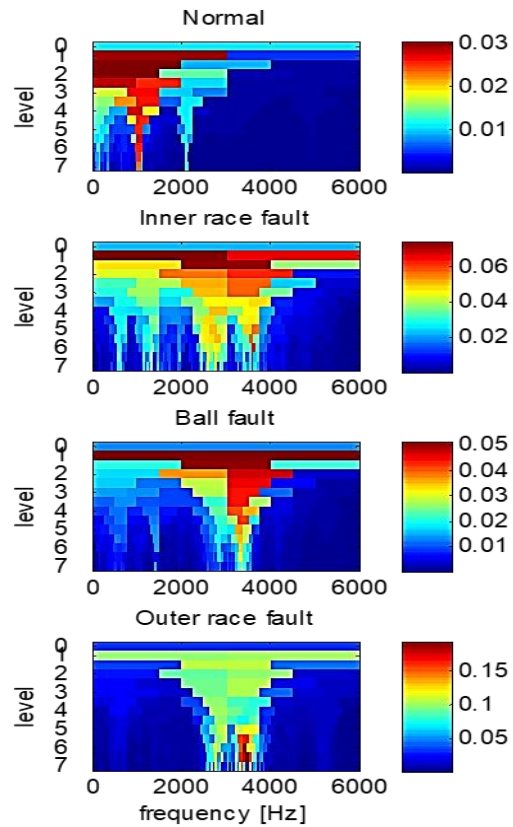


Figure 3. The Fast Kurtogram using harmmean feature

5. Conclusion

In this paper, based on the technique of Fast Kurtogram, the novel technique was introduced on other types of statistical features instead of the Kurtosis for the first time. To this purpose, we examined the issue of four classes of Bearing Fault Detection by using 20 different statistical features. This study was conducted in four stages. At first, the stability of each feature was checked for each failure. Then resistance to load change and failure growth was studied. In the end, the resolution and fault detection for each feature was calculated. From the above results, the best feature, which was both resistant and repeatable to different variations, as well as accurate detection and resolution was selected, and it was found that the Kurtosis is not well-positioned in comparison with other statistical attributes such as harmmean and median. In this research that was done based on kurtogram method, in fact instead of using kurtosis feature, other statistical features were utilized. In future work, it can be implemented that instead of using time signal in the frequency bounds, at the first the signal processing methods will be applied, then kurtosis feature will be calculated from signal processing, and the result will be compared with the kurtogram method.

References

[1] H. Yang, J. Mathew, L. Ma, Fault diagnosis of rolling element bearings using basis pursuit, *Mechanical Systems and Signal Processing*, Vol. 19, No. 2, pp. 341-356, 2005/03/01/, 2005.

[2] M. Liang, I. Soltani Bozchalooi, An energy operator approach to joint application of amplitude and frequency-demodulations for bearing fault detection, *Mechanical Systems and Signal Processing*, Vol. 24, No. 5, pp. 1473-1494, 2010/07/01/, 2010.

- [3] W. Su, F. Wang, H. Zhu, Z. Zhang, Z. Guo, Rolling element bearing faults diagnosis based on optimal Morlet wavelet filter and autocorrelation enhancement, *Mechanical Systems and Signal Processing*, Vol. 24, No. 5, pp. 1458-1472, 2010/07/01/, 2010.
- [4] D. Dou, J. Yang, J. Liu, Y. Zhao, A rule-based intelligent method for fault diagnosis of rotating machinery, *Knowledge-Based Systems*, Vol. 36, pp. 1-8, 2012/12/01/, 2012.
- [5] B. Li, P.-y. Liu, R.-x. Hu, S.-s. Mi, J.-p. Fu, Fuzzy lattice classifier and its application to bearing fault diagnosis, *Applied Soft Computing*, Vol. 12, No. 6, pp. 1708-1719, 2012/06/01/, 2012.
- [6] D. Wang, P. W. Tse, K. L. Tsui, An enhanced Kurtogram method for fault diagnosis of rolling element bearings, *Mechanical Systems and Signal Processing*, Vol. 35, No. 1, pp. 176-199, 2013/02/01/, 2013.
- [7] H. Xu, G. Chen, An intelligent fault identification method of rolling bearings based on LSSVM optimized by improved PSO, *Mechanical Systems and Signal Processing*, Vol. 35, No. 1, pp. 167-175, 2013/02/01/, 2013.
- [8] H. Al-Bugharbee, I. Trendafilova, A fault diagnosis methodology for rolling element bearings based on advanced signal pretreatment and autoregressive modelling, *Journal of Sound and Vibration*, Vol. 369, pp. 246-265, 2016/05/12/, 2016.
- [9] P. Baraldi, F. Cannarile, F. Di Maio, E. Zio, Hierarchical k-nearest neighbours classification and binary differential evolution for fault diagnostics of automotive bearings operating under variable conditions, *Engineering Applications of Artificial Intelligence*, Vol. 56, pp. 1-13, 2016/11/01/, 2016.
- [10] V. Vakharia, V. K. Gupta, P. K. Kankar, Bearing Fault Diagnosis Using Feature Ranking Methods and Fault Identification Algorithms, *Procedia Engineering*, Vol. 144, pp. 343-350, 2016/01/01/, 2016.
- [11] J. Singh, A. K. Darpe, S. P. Singh, Rolling element bearing fault diagnosis based on Over-Complete rational dilation wavelet transform and auto-correlation of analytic energy operator, *Mechanical Systems and Signal Processing*, Vol. 100, pp. 662-693, 2018/02/01/, 2018.
- [12] M. Ö. Yaylı, Stability analysis of gradient elastic microbeams with arbitrary boundary conditions, *Journal of Mechanical Science and Technology*, Vol. 29, No. 8, pp. 3373-3380, 2015/08/01, 2015.
- [13] M. Özgür Yaylı, An efficient solution method for the longitudinal vibration of nanorods with arbitrary boundary conditions via a hardening nonlocal approach, *Journal of Vibration and Control*, Vol. 24, No. 11, pp. 2230-2246, 2018/06/01, 2016.
- [14] M. Ö. Yaylı, Buckling analysis of a microbeam embedded in an elastic medium with deformable boundary conditions, *Micro & Nano Letters*, Vol. 11, No. 11, pp. 741-745, 2016.
- [15] M. Ö. Yaylı, On the torsional vibrations of restrained nanotubes embedded in an elastic medium, *Journal of the Brazilian Society of Mechanical Sciences and Engineering*, Vol. 40, No. 9, pp. 419, 2018/08/14, 2018.
- [16] M. Ö. Yaylı, Torsional vibrations of restrained nanotubes using modified couple stress theory, *Microsystem Technologies*, Vol. 24, No. 8, pp. 3425-3435, 2018/08/01, 2018.
- [17] A. Moradi, H. Makvandi, I. B. Salehpoor, Multi objective optimization of the vibration analysis of composite natural gas pipelines in nonlinear thermal and humidity environment under non-uniform magnetic field, *JOURNAL OF COMPUTATIONAL APPLIED MECHANICS*, Vol. 48, No. 1, pp. 53-64, 2017.
- [18] P. Alimouri, S. Moradi, R. Chinipardaz, UPDATING FINITE ELEMENT MODEL USING FREQUENCY DOMAIN DECOMPOSITION METHOD AND BEES ALGORITHM, *THE JOURNAL OF COMPUTATIONAL APPLIED MECHANICS*, Vol. 48, No. 1, pp. 75-88, 2017. English
- [19] M. Goodarzi, M. N. Bahrani, V. Tavaf, Refined plate theory for free vibration analysis of FG nanoplates using the nonlocal continuum plate model, *Journal of Computational Applied Mechanics*, Vol. 48, No. 1, pp. 123-136, 2017.
- [20] A. Zargaripoor, A. Bahrani, M. Nikkhah bahrani, Free vibration and buckling analysis of third-order shear deformation plate theory using exact wave propagation approach, *Journal of Computational Applied Mechanics*, Vol. 49, No. 1, pp. 102-124, 06/01, 2018. en
- [21] A. Zargaripoor, M. Nikkhah bahrani, A wave-based computational method for free vibration and buckling analysis of rectangular Reddy nanoplates, *Journal of Computational Applied Mechanics*, 05/23, 2018. en
- [22] M. Zarchi, B. Attaran, Performance improvement of an active vibration absorber subsystem for an aircraft model using a bees algorithm based on multi-objective intelligent optimization, *Engineering Optimization*, Vol. 49, No. 11, pp. 1905-1921, 2017/11/02, 2017.
- [23] M. Zarchi, B. Attaran, Improved design of an active landing gear for a passenger aircraft using multi-objective optimization technique, *Structural and Multidisciplinary Optimization*, Vol. 59, No. 5, pp. 1813-1833, 2019/05/01, 2019.
- [24] S. Patil, V. Phalle, Fault Detection of Anti-friction Bearing using Ensemble Machine Learning Methods, *International Journal of Engineering*, Vol. 31, No. 11, pp. 1972-1981, 2018. En
- [25] M. Heidari, Fault Detection of Bearings Using a Rule-based Classifier Ensemble and Genetic Algorithm, *International Journal of Engineering, Transactions A: Basics*, Vol. 30, pp. 604-609, 04/01, 2017.
- [26] X. Li, L. Han, H. Xu, Y. Yang, H. Xiao, Rolling bearing fault analysis by interpolating windowed DFT algorithm, *International Journal of Engineering, Transactions A: Basics*, Vol. 32, pp. 121-126, 01/01, 2019.
- [27] A. Moshrefzadeh, A. Fasana, The Autogram: An effective approach for selecting the optimal demodulation band in rolling element bearings diagnosis, *Mechanical Systems and Signal Processing*, Vol. 105, pp. 294-318, 2018/05/15/, 2018.
- [28] J. Antoni, The spectral kurtosis of nonstationary signals: Formalisation, some properties, and application, in *Proceeding of*, 1167-1170.
- [29] Diagnostic Techniques, *Vibration-based Condition Monitoring*, pp. 167-227, 2010/12/19, 2010.
- [30] J. Antoni, R. B. Randall, The spectral kurtosis: application to the vibratory surveillance and diagnostics of rotating machines, *Mechanical Systems and Signal Processing*, Vol. 20, No. 2, pp. 308-331, 2006/02/01/, 2006.
- [31] J. Antoni, Fast computation of the kurtogram for the detection of transient faults, *Mechanical Systems and Signal Processing*, Vol. 21, No. 1, pp. 108-124, 2007/01/01/, 2007.